3D SURFACE RECONSTRUCTION BASED ON COMBINED ANALYSIS OF REFLECTANCE AND POLARISATION PROPERTIES: A LOCAL APPROACH

Pablo d'Angelo and Christian Wöhler

DaimlerChrysler Research and Technology, Machine Perception
P. O. Box 2360, D-89013 Ulm, Germany

KEY WORDS: surface reconstruction, polarization vision, shape from shading, quality inspection

ABSTRACT

An image-based 3D surface reconstruction technique based on simultaneous evaluation of reflectance and polarisation features is introduced in this paper. The proposed technique is suitable for single and multi-image (photopolarimetric stereo) analysis. It is especially suited for the difficult task of 3D reconstruction of rough metallic surfaces with non-Lambertian reflectance. The reflectance and polarisation properties are used to determine the surface gradients individually for each image pixel. The presented multi-image technique is invariant to variations of the surface albedo. We evaluate our algorithm based on synthetic ground truth data as well as on a raw forged iron surface. The results we obtain for the real world example demonstrate the applicability of our method in the domain of industrial quality inspection.

1 INTRODUCTION

Three-dimensional reconstruction of surfaces has become an important technique in the context of industrial quality inspection. In the field of optical metrology, the currently most widely used active approaches are primarily based on *projection of structured light* (Batlle et al., 1998). While such methods are accurate, they require a highly precise mutual calibration of cameras and structured light sources. Multiple structured light sources may be needed for 3D reconstruction of non-convex surfaces. Hence, for inline quality inspection of industrial part surfaces, less intricate passive image-based techniques are desirable.

A well-known passive image-based surface reconstruction method is *shape from shading*. This approach aims at deriving the orientation of the surface at each pixel by using a model of the reflectance properties of the surface and knowledge about the illumination conditions (Horn and Brooks, 1989). The integration of shadow information into the shape from shading formalism and applications of such methods in the context of fast inline quality inspection have been demonstrated (Wöhler and Hafezi, 2005).

A further approach to reveal the 3D shape of a surface is to utilise polarisation data. Most current literature concentrates on dielectric surfaces, as for smooth dielectric surfaces, the direction and degree of polarisation as a function of surface orientation are governed by elementary physical laws (Miyazaki et al., 2004). For smooth dielectric surfaces a 3D surface reconstruction framework is proposed relying on the analysis of the polarisation state of reflected light, the surface texture, and the locations of specular reflections (Miyazaki et al., 2003). In previous work, reflectance and polarisation properties of metallic surfaces are examined, but no physically motivated polarisation model is derived (Wolff, 1991). Furthermore, it has been demonstrated that polarisation information can be used to determine surface orientation (Rahmann and Canterakis, 2001). Applications of such *shape from polarisation* approaches to real-world scenarios, however, are rarely described in the literature. A variational combined shape from shading and polarisation algorithm relying on the minimisation of a global error function is introduced in (d'Angelo and Wöhler, 2005) and applied to 3D reconstruction of metallic surfaces.

In this paper we present an image-based method for 3D surface reconstruction by simultaneous evaluation of information about reflectance and polarisation. This method will be applied relying on a pair of polarisation images of the surface (*photopolarimetric stereo*). It is assumed that the scene is illuminated by unpolarised point light sources situated at known locations. The reflectance and polarisation properties of the surface material are measured over a wide range of surface orientations by evaluating a series of images acquired through a linear polarisation filter under different rotation angles, respectively. Parameterised phenomenological models will then be fitted to the obtained measurements. Both reflectance and polarisation features are used to determine the surface gradient individually for each image pixel, without introducing global constraints like smoothness (d'Angelo and Wöhler, 2005).

We systematically evaluate our method on a synthetically generated surface in order to examine its accuracy, convergence behaviour, and noise-robustness. We furthermore investigate the accuracy of our 3D reconstruction technique for the real-world example of a raw forged iron surface.

2 REFLECTANCE AND POLARISATION MODELS

2.1 Measurement of reflectance properties

The pixel intensity $I(u, v)$ observed by a camera is governed by the *reflectance function* of the surface material,

$$I(u, v) = R\left(\vec{n}(u, v), \vec{s}, \vec{v}\right), \tag{1}$$

which depends on the surface normal $\vec{n}$, the illumination direction $\vec{s}$, and the direction $\vec{v}$ to the camera. We assume that both light source and camera are situated at infinite distance from the object, such that $\vec{s}$ and $\vec{v}$ are assumed to be constant. In the following, the surface normal $\vec{n}$ will be represented in *gradient space* by the directional derivatives $p = z_x$ and $q = z_y$ of the surface function $z(x, y)$ with $\vec{n} = (-p, -q, 1)^T$. We define accordingly $\vec{s} = (-p_s, -q_s, 1)^T$ and $\vec{v} = (-p_v, -q_v, 1)^T$ in gradient space.

A well-known special case is the Lambertian reflectance function $R\left(\vec{n}, \vec{s}\right) = \rho(u, v) \cos\theta_i$ with $\cos\theta_i = \vec{n} \cdot \vec{s} / \left(|\vec{n}||\vec{s}|\right)$ and $\rho(u, v)$ as the *surface albedo*. In this paper, however, we regard

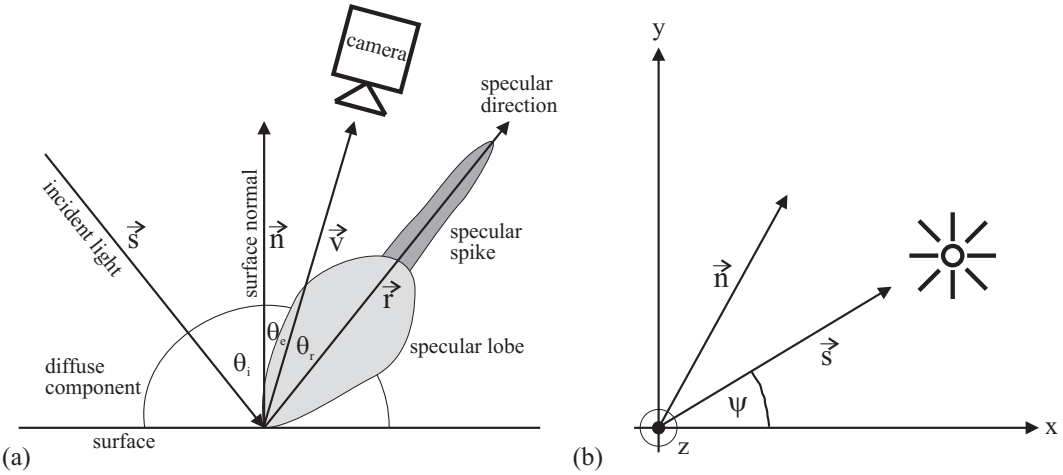

Figure 1: (a) Plot of the three reflectance components. (b) Definition of the world coordinate system and the azimuth angle ψ.

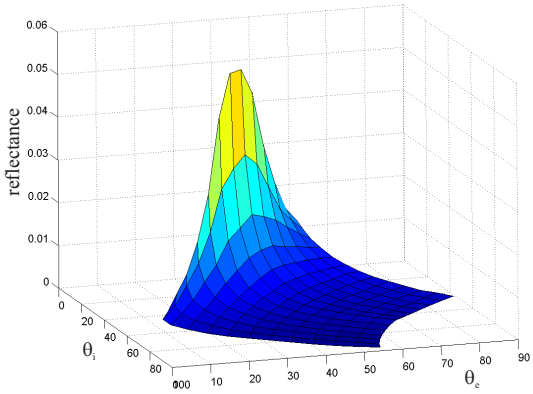

Figure 2: Left: Measured reflectance of a raw forged iron surface for $\alpha = 75°$. The parameters of the reflectance function (cf. Eq. 2) amount to $\sigma_1 = 3.85$, $m_1 = 2.61$, $\sigma_2 = 9.61$, and $m_2 = 15.8$, where the specular lobe is described by σ_1 and m_1 and the specular spike by σ_2 and m_2.

metallic surfaces with a strongly non-Lambertian reflectance behaviour. We will assume that the reflectance of a typical rough metallic surface consists of three components: a diffuse (Lambertian) component, the *specular lobe*, and the *specular spike* (Nayar et al., 1991). The diffuse component is generated by internal multiple scattering processes. The specular lobe, which is caused by single reflection at the surface, is distributed around the specular direction and may be rather broad. The specular spike is concentrated in a small region around the specular direction and represents mirror-like reflection, which is dominant in the case of smooth surfaces. Fig. 1a illustrates the three components of the reflectance function. We define an analytical form for the reflectance for which we perform a least-mean-squares fit to the measured reflectance values, depending on the incidence angle θ_i, the angle θ_r between the specular direction $\vec{r}$ and the viewing direction $\vec{v}$ (cf. Fig. 1a), and the phase angle α between the vectors $\vec{s}$ and $\vec{v}$:

$$R(\theta_i, \theta_r, \alpha) = \rho \left[\cos\theta_i + \sum_{n=1}^{N} \sigma_n \cdot (\cos\theta_r)^{m_n} \right]. \quad (2)$$

The angle θ_r can be expressed in terms of incidence angle, emission angle, and phase angle according to

$$\cos\theta_r = 2\cos\theta_i \cos\theta_e - \cos\alpha, \quad (3)$$

such that our phenomenological reflectance model only depends on the incidence angle θ_i, the emission angle θ_e, and the phase angle α. Note that $\alpha \leq \theta_i + \theta_e$ in the general three-dimensional case. For $\theta_r > 90°$ only the diffuse component is considered. The albedo ρ is assumed to be constant over the surface. The shapes of the specular components of the reflectance function are approximated by $N = 2$ terms proportional to powers of $\cos\theta_r$. The coefficients $\{\sigma_n\}$ denote the strength of the specular components relative to the diffuse component, while the parameters $\{m_n\}$ denote their widths. All introduced phenomenological parameters generally depend on the phase angle α. For our measurements we use a goniometer to adjust the angles θ_i and θ_e. The phase angle α between the vectors $\vec{s}$ and $\vec{v}$ is assumed to be constant over the image.

For each configuration of θ_i, θ_e, and α, we acquire a high dynamic range image by combining several images taken with different shutter times. The reflectance of the sample surface under the given illumination conditions is then obtained by computing the average greyvalue over an area in the high dynamic range image that contains a flat part of the sample surface. A reflectance measurement typical for raw forged or cast iron surfaces is shown in Fig. 2 for $\alpha = 75°$.

2.2 Measurement of polarisation properties

In our scenario, the incident light is unpolarised. For smooth metallic surfaces the light remains unpolarised after reflection at the surface. Rough metallic surfaces, however, partially polarise the reflected light (Wolff, 1991). The measurement of the polarisation properties of the surface is similar to the reflectance measurement. For each configuration of goniometer angles, five high dynamic range images are acquired through a linear polarisation filter at multiple orientation angles ω between $0°$ and $180°$. For each filter orientation ω, an average pixel intensity over an image area containing a flat part of the sample surface is computed as described in Section 2.1. To the measured pixel intensities we fit a sinusoidal function (Wolff, 1991) of the form

$$I(\omega) = I_c + I_v \cos(\omega - \Phi). \quad (4)$$

The filter orientation Φ for which maximum intensity $I_c + I_v$ is observed corresponds to the *polarisation angle* ($\omega = \Phi$). The *polarisation degree* amounts to $D = I_v / I_c$. In principle, three measurements would be sufficient to determine the three parameters I_c, I_v, and Φ, but the fit becomes less noise-sensitive and thus more accurate when more measurements are used. The parameter I_c represents the reflectance of the surface.

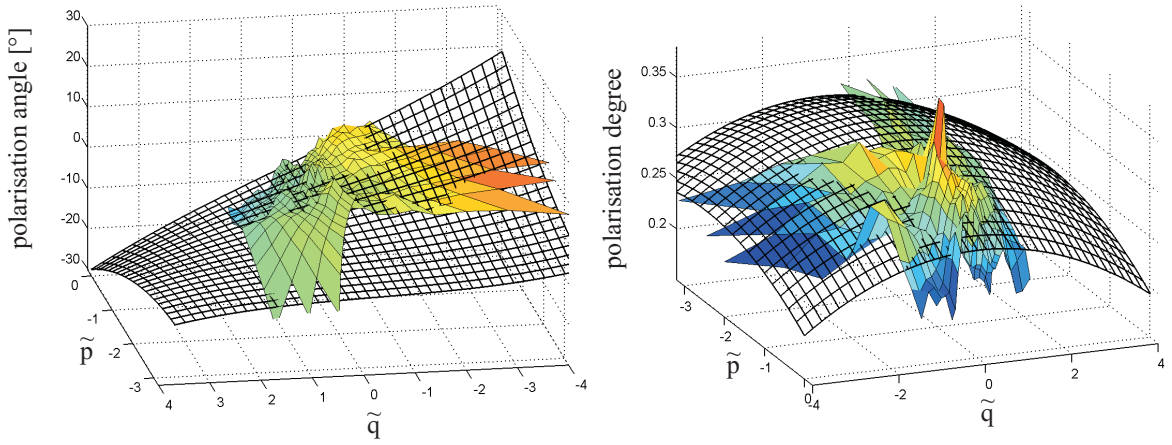

Figure 3: Measured and modelled polarisation properties of a raw forged iron surface. Left: polarisation angle. Right: polarisation degree.

According to Fig. 1b, the rotation angles of the goniometer define the surface normal $\tilde{\vec{n}} = (-\tilde{p}, -\tilde{q}, 1)$ of the sample surface in a coordinate system with positive x and zero y component of the illumination vector $\vec{s}$, corresponding to $p_s < 0$ and $q_s = 0$. Without loss of generality we will in the following assume a viewing direction $\vec{v} = (0, 0, 1)^T$. The surface normal $\vec{n}$ in the world coordinate system, in which the azimuth angle of the light source is denoted by the angle ψ, is related to $\tilde{\vec{n}}$ by a rotation $R_z(\psi)$ around the z axis, leading to

$$\begin{aligned} \tilde{p} &= p\cos\psi + q\sin\psi \\ \tilde{q} &= -p\sin\psi + q\cos\psi. \end{aligned} \tag{5}$$

Due to the lack of an accurate physically motivated model for the polarisation properties of rough metallic surfaces, we perform a polynomial fit in terms of the surface gradients $\tilde{p}$ and $\tilde{q}$ to the measured values of the polarisation angle Φ and degree D. In this framework, the modelled polarisation angle R_Φ is represented by an incomplete third-degree polynomial of the form

$$R_\Phi(\tilde{p}, \tilde{q}) = a_\Phi + b_\Phi\tilde{p}\tilde{q} + c_\Phi\tilde{q} + d_\Phi\tilde{p}^2\tilde{q} + e_\Phi\tilde{q}^3. \tag{6}$$

The constant offset a_Φ can be made zero by correspondingly defining the zero position of the orientation angle ω of the linear polarisation filter. Eq. (6) is antisymmetric in $\tilde{q}$ with respect to a_Φ. At the same time, $R_\Phi(\tilde{p}, \tilde{q}) = a_\Phi = \text{const}$ for $\tilde{q} = 0$, corresponding to coplanar vectors $\vec{n}$, $\vec{s}$, and $\vec{v}$. These properties are required for geometrical symmetry reasons as long as the interaction between the incident light and the surface material can be assumed to be isotropic.

The observed polarisation degree R_D is represented in an analogous manner by an incomplete second-degree polynomial of the form

$$R_D(\tilde{p}, \tilde{q}) = a_D + b_D\tilde{p} + c_D\tilde{p}^2 + d_D\tilde{q}^2. \tag{7}$$

In this case, symmetry in $\tilde{q}$ is imposed for geometrical reasons, once more due to the assumed isotropy of light-surface interaction. Fig. 3 illustrates the polarisation properties of a raw forged iron surface at a phase angle of $\alpha = 75°$ along with the polynomial fits according to Eqs. (6) and (7).

3 3D SURFACE RECONSTRUCTION USING REFLECTANCE AND POLARISATION

Well-known approaches to reflectance-based 3D surface reconstruction are *shape from shading* and *photometric stereo*, the latter term referring to the evaluation of multiple images of the surface acquired under different illumination conditions. These methods aim at determining the surface gradient field, which is then integrated in order to obtain the depth $z(u, v)$. In this section we will extend this approach by introducing polarisation information.

The reflectance function as well as polarisation angle and degree can be expressed in terms of the surface gradients $p(u, v)$ and $q(u, v)$:

$$I(u,v) = R\left(p(u,v), q(u,v)\right) \tag{8}$$

$$\Phi(u,v) = R_\Phi\left(p(u,v), q(u,v)\right) \tag{9}$$

$$D(u,v) = R_D\left(p(u,v), q(u,v)\right) \tag{10}$$

The representation of R in Eq. (8) is called *reflectance map* (Horn and Brooks, 1989). Provided that the model parameters of the reflectance and polarisation functions R, R_Φ, and R_D are known and measurements of intensity and polarisation properties are available for each image pixel, the surface gradients p and q can be obtained by solving the nonlinear system of equations (8)–(10). For this purpose we make use fo the Levenberg-Marquardt algorithm in the overdetermined case and the Powell dogleg method (Powell, 1970) otherwise. In the overdetermined case, the root of Eqs. (8)-(10) is determined in the least-mean-squares sense. The contributions from the different terms are then weighted according to the measurement errors, respectively, which we have determined to $\sigma_I = 10^{-3} I_{\text{spec}}$ with I_{spec} as the intensity of the specular reflections, $\sigma_\Phi = 0.2°$ and $\sigma_D = 0.01$. The surface profile $z(u, v)$ is derived from the resulting gradients $p(u, v)$ and $q(u, v)$ by means of numerical integration of the gradient field (Jiang and Bunke, 1997).

It is straightforward to extend this approach to photopolarimetric stereo because each light source provides an additional set of equations. Eq. (8) can only be solved, however, when the surface albedo $\rho(u, v)$ is known for each surface point. A constant albedo can be assumed in many applications. If this assumption is not valid, albedo variations will affect the accuracy of surface reconstruction.

For surfaces with unknown and non-uniform albedo it is possible to utilise two images acquired under different illumination conditions, such that Eq. (8) can be replaced by

$$\frac{I_1}{I_2} = \frac{R_1\left(p(u,v), q(u,v)\right)}{R_2\left(p(u,v), q(u,v)\right)} \tag{11}$$

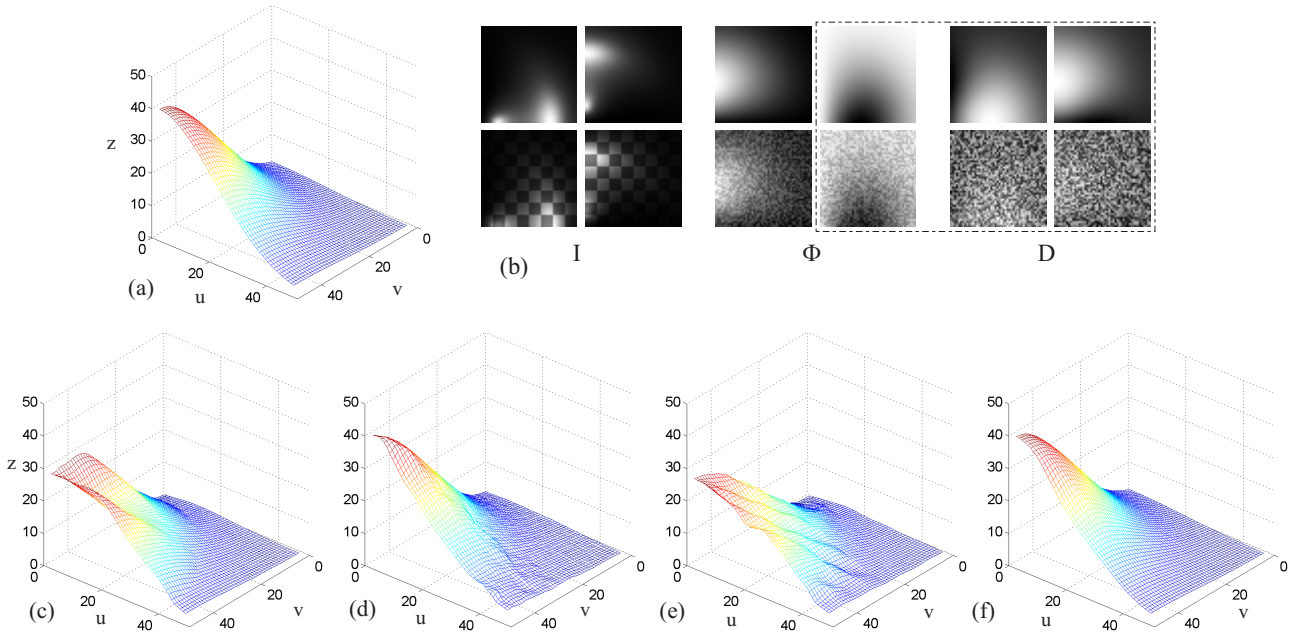

Figure 4: 3D reconstruction of a synthetically generated surface based on a photopolarimetric stereo image pair. (a) Ground truth. (b) From the left: Reflectance, polarisation angle and degree images, without and with non-uniform albedo, without and with noise, respectively (cf. Table 1). The second polarisation angle image and both polarisation degree images have been excluded from the analysis (cf. Section 4.1). Reconstruction result for noisy images of a surface with uniform albedo is shown in (c) using the albedo-dependent approach according to Eq. (8) and in (d) using the albedo-independent approach according to Eq. (11). Reconstruction results for a surface with non-uniform albedo in the noise-free case is shown in (e) for the albedo-dependent and in (f) for the albedo-independent approach.

In Eq. (11), the albedo cancels out. The quotient approach has been introduced in the context of photoclinometric analysis of planetary surfaces (McEwen, 1985) and has been integrated into the shape from shading formalism (Wöhler and Hafezi, 2005).

An advantage of the described local approach is that the 3D reconstruction result is not affected by additional constraints such as smoothness of the surface but directly yields the surface gradient field for each image pixel. A drawback, however, is the fact that due to the inherent nonlinearity of the problem, existence and uniqueness of a solution for p and q are not guaranteed for both the albedo-dependent and the albedo-independent case. But in the experiments presented in Section 4 we show that in practically relevant scenarios a reasonable solution for the surface gradient field and the resulting depth $z(u, v)$ is obtained even in the presence of noise.

4 EXPERIMENTAL RESULTS

4.1 Evaluation based on synthetic ground truth data

To examine the accuracy of 3D reconstruction, we apply the algorithm described in Section 3 to the synthetically generated surface shown in Fig. 4a. We still assume a perpendicular view on the surface along the z axis, corresponding to $\vec{v} = (0, 0, 1)^T$. The scene is illuminated by $L = 2$ light sources (one after the other) under an angle of 15° with respect to the horizontal plane at azimuth angles of $\psi^{(1)} = 0^\circ$ and $\psi^{(2)} = 90^\circ$, respectively. This setting results in identical phase angles $\alpha^{(1)} = \alpha^{(2)} = 75^\circ$ for the two light sources. The initial values for $p(u, v)$ and $q(u, v)$ must be provided relying on a-priori knowledge about the surface orientation. In the synthetic surface example, they are initialised with the value -0.5. It has been demonstrated that the initial gradients can be estimated using depth from defocus (d'Angelo and Wöhler, 2005).

The synthetic reflectance and polarisation angle images shown in Fig. 4b have been generated by means of the polynomial fits to the measured reflectance and polarisation properties presented in Figs. 2 and 3. We have used two synthetic surfaces for an evaluation of our reconstruction method, one surface with uniform albedo and one with spatially non-uniform albedo. In our experiments we have found that the behaviour of the polarisation degree of rough metallic surfaces tends to change significantly over the surface, due to local variations of the surface roughness (d'Angelo and Wöhler, 2005). In contrast, the behaviour of the polarisation angle does not show local variations over the surface. We thus decided not to make use of the polarisation degree in our practical experiments (cf. Section 4.2).

According to Fig. 3, the observed polarisation angles cover only a narrow interval. Hence, we have observed that the azimuth angle ψ must be known at an accuracy of about 0.1° if one desires to use both polarisation angle images for reconstruction, while the reflectance is less sensitive in this respect. As such accurate knowledge of ψ is difficult to obtain for practical reasons, we decided to use only one polarisation angle image.

The reconstruction results are shown in Fig. 4. The noise level amounts to 5 times the measurement errors given in Section 3. The corresponding RMS deviations from the ground truth for z, p, and q are given in Table 1. We have observed that for a significant fraction of pixels (about 25 percent) no solution of Eqs. (8)–(9) is obtained with the applied initialisation, presumably due to a small convergence radius. When Eq. (8) is replaced by Eq. (11), convergence is achieved for all pixels, leading to much higher accuracy of reconstruction. We have found experimentally that it is possible to decrease the reconstruction error obtained from Eq. (8) by decreasing the weight of the reflectance in the least-mean-squares optimisation. As seen from the RMS error of z, the quotient-based approach according to Eq. (11) yields the same re-

Table 1: Evaluation results on the synthetic ground truth example shown in Fig. 4 using both reflectance images but only one polarisation angle image.

Method	Albedo	RMS error (without noise)			RMS error (with noise)		
		z	p	q	z	p	q
I_1,I_2,Φ_1	uniform	3.2	0.20	0.18	3.2	0.20	0.19
I_1,I_2,Φ_1	non-uniform	4.1	0.25	0.24	4.1	0.26	0.24
I_1/I_2,Φ_1	uniform	0.4	0.10	0.00	0.8	0.24	0.16
I_1/I_2,Φ_1	non-uniform	0.4	0.10	0.00	0.8	0.24	0.17

Table 2: Evalutation results on synthetic ground truth data using various combinations of all available reflectance and polarisation data.

Method	Albedo	RMS error (without noise)			RMS error (with noise)		
		z	p	q	z	p	q
I_1,Φ_1	uniform	0.7	0.15	0.01	1.3	0.19	0.16
I_1,Φ_1	non-uniform	1.5	0.21	0.04	1.5	0.22	0.16
I_1,D_1	uniform	0.5	0.01	0.11	9.1	0.85	1.10
I_1,D_1	non-uniform	2.5	0.11	0.42	7.7	0.82	1.17
Φ_1,D_1	uniform	0.0	0.00	0.00	4.0	1.10	0.29
Φ_1,D_1	non-uniform	0.0	0.00	0.00	4.0	1.10	0.29
I_1,Φ_1,D_1	uniform	0.5	0.13	0.01	1.4	0.22	0.16
I_1,Φ_1,D_1	non-uniform	1.4	0.20	0.04	1.3	0.24	0.16
I_1,I_2	uniform	3.6	0.26	0.26	3.6	0.27	0.27
I_1,I_2	non-uniform	4.1	0.33	0.33	4.1	0.32	0.31
I_1,I_2,Φ_1,Φ_2	uniform	2.7	0.17	0.17	2.8	0.18	0.18
I_1,I_2,Φ_1,Φ_2	non-uniform	4.0	0.25	0.25	4.0	0.24	0.24
I_1,I_2,D_1,D_2	uniform	3.6	0.21	0.21	3.6	0.21	0.21
I_1,I_2,D_1,D_2	non-uniform	4.1	0.26	0.26	4.1	0.26	0.26
I_1,I_2,Φ_1,Φ_2,D_1,D_2	uniform	2.7	0.17	0.17	2.7	0.18	0.17
I_1,I_2,Φ_1,Φ_2,D_1,D_2	non-uniform	4.0	0.25	0.25	4.0	0.24	0.24
I_1/I_2,Φ_1,Φ_2	uniform	0.0	0.00	0.00	0.2	0.12	0.12
I_1/I_2,Φ_1,Φ_2	non-uniform	0.0	0.00	0.00	0.2	0.12	0.12
I_1/I_2,Φ_1,Φ_2,D_1,D_2	uniform	0.0	0.00	0.00	0.2	0.12	0.11
I_1/I_2,Φ_1,Φ_2,D_1,D_2	non-uniform	0.0	0.00	0.00	0.2	0.12	0.12

sults for the surfaces with uniform and non-uniform albedo, while the error increases when Eq. (8), assuming a uniform albedo, is used.

For comparison, we report in Table 2 the reconstruction accuracy obtained using various combinations of all available reflectance and polarisation data, including the polarisation degree. The values are computed both for a single set and for a pair of reflectance and polarisation images, respectively. We have found that a pair of intensity images alone is not sufficient for reasonably accurate 3D surface reconstruction. With both reflectance and polarisation angle images, the reconstruction results become virtually exact when Eq. (11) is used. Even with a single light source we obtain good reconstruction results when all available reflectance and polarisation data are used.

4.2 Application to a rough metallic surface

We will now describe the application of our photopolarimetric 3D reconstruction method to the raw forged iron surface of an automotive part. Image resolution was 0.30 mm per pixel. For each pixel, the polarisation properties are determined as described in Section 2. The 3D reconstruction result $z(u, v)$ along with the reflectance and polarisation images is shown in Fig. 5 for a flawless and a deformed part, respectively. As discussed in Section 4.1, the reconstruction is based on the quotient I_1/I_2 of the two reflectance images and one polarisation angle image. The surface gradients $p(u, v)$ and $q(u, v)$ are initialised with zero values. The difference between the two surfaces shows that some material is missing in the deformed part. This is due to a fault caused during the forging process. The offset between the two surfaces at the margin of the part amounts to 2.05 ± 0.05 mm along the surface normal, obtained by tactile measurement with a sliding calliper at the points indicated by the arrows in Fig. 5b. The 3D reconstruction yields a value of 2.1 mm (Fig. 5c), which is in good agreement. A cross-section of the same surface was measured with a laser focus profilometer and compared to the corresponding cross-section extracted from the reconstructed 3D profile (Fig. 5d). The RMS deviation amounts to 0.22 mm, corresponding to about two-thirds of a pixel.

5 SUMMARY AND CONCLUSION

In this paper we have presented an image-based method for 3D surface reconstruction relying on the simultaneous evaluation of reflectance and polarisation information for multiple images (photopolarimetric stereo). The reflectance and polarisation properties of the surface material have been obtained by means of a series of images acquired through a linear polarisation filter under different orientations. Analytic phenomenological models have been fitted to the obtained measurements, allowing for an integration of both reflectance and polarisation features into a unified local (pixel-wise) optimisation framework. The presented method has been evaluated based on a synthetically generated surface. The dependence of the accuracy of 3D reconstruction on the utilised reflectance and polarisation data is systematically examined. Furthermore we have applied our method to the difficult real-world scenario of 3D reconstruction of a surface section of a raw forged iron part. We have shown that our approach is suitable

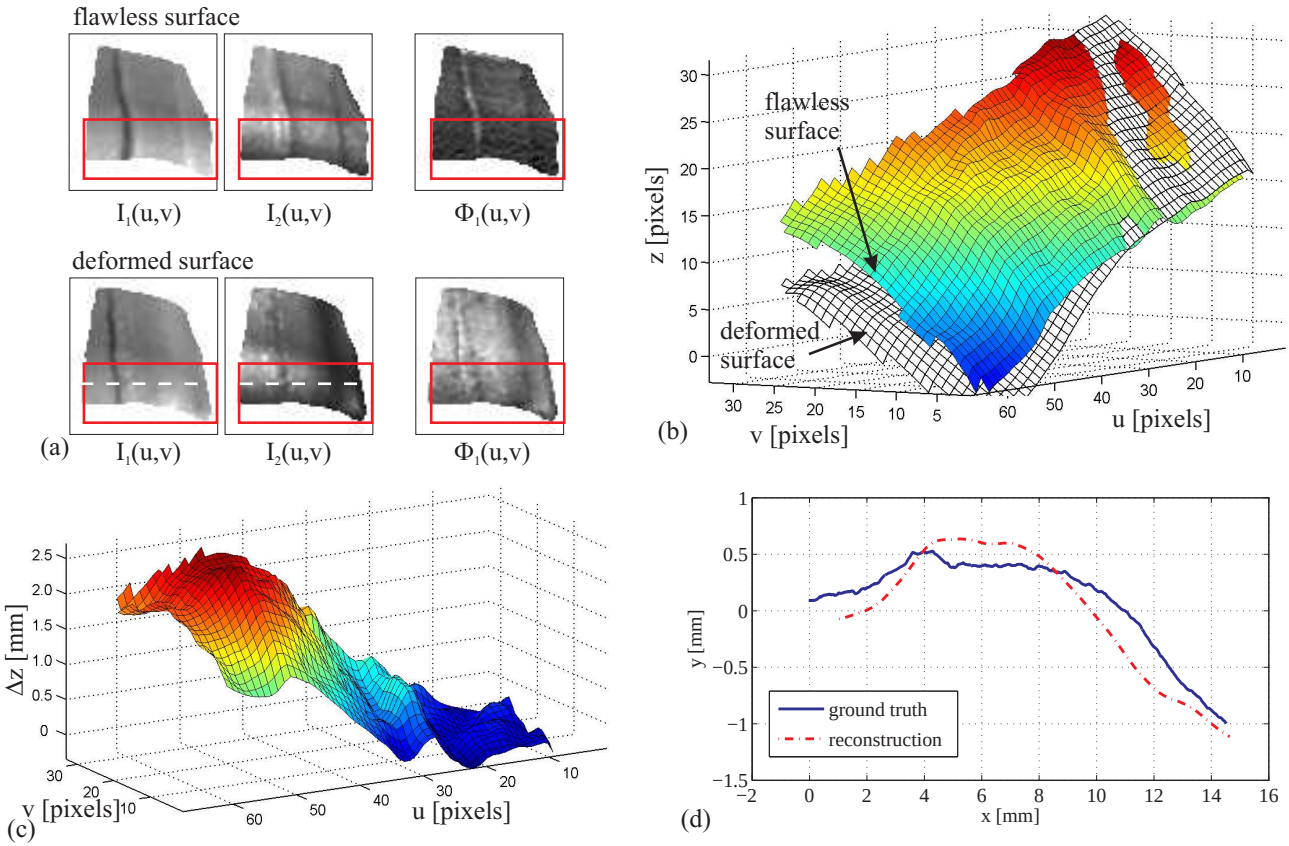

Figure 5: Application of the described 3D surface reconstruction method to a raw forged iron surface. (a) Reflectance and polarisation angle images. The red boxes indicate the reconstructed area. (b) Reconstructed 3D profiles of both parts, viewed from the upper right. (c) Difference Δz between flawless and deformed surface. (d) Comparison of the cross-section indicated by the dashed line in (a) to ground truth.

for detecting anomalies of the surface shape, thus rendering it a promising technique for optical quality inspection systems.

REFERENCES

Batlle, J., Mouaddib, E., Salvi, J., 1998. Recent progress in coded structured light as a technique to solve the correspondence problem: a survey. *Pattern Recognition*, 31(7), pp. 963-982.

D'Angelo, P., Wöhler, C., 2005. 3D Reconstruction of Metallic Surfaces by Photopolarimetric Analysis. In: H. Kalviainen et al. (Eds.), *Proc. 14th Scand. Conf. on Image Analysis*, LNCS 3540, Springer-Verlag Berlin Heidelberg, pp. 689-698.

D'Angelo, P., Wöhler, C., 2005. 3D Surface Reconstruction by Combination of Photopolarimetry and Depth from Defocus. *Pattern Recognition, Proc. of 27th DAGM Symposium*, LNCS 3663, Springer-Verlag Berlin Heidelberg, pp. 176-183.

Horn, B. K. P., Brooks, M. J., 1989. *Shape from Shading*. MIT Press, Cambridge, Massachusetts.

Horn, B. K. P., 1989. Height and Gradient from Shading. MIT technical report 1105A. http://people.csail.mit.edu/people/bkph/AIM/AIM-1105A-TEX.pdf

Jiang, X., Bunke, H., 1997. *Dreidimensionales Computersehen*. Springer-Verlag, Berlin.

McEwen, A.S., 1985. Topography and albedo of Ius Chasma, Mars. *Proc. 16th Conf. on Lunar and Planetary Science*, pp. 528-529.

Miyazaki, D., Kagesawa, M., Ikeuchi, K., 2004 Transparent Surface Modeling from a Pair of Polarization Images. *IEEE Trans. on Pattern Analysis and Machine Intelligence*, 26(1), pp. 73-82.

Miyazaki, D., Tan, R. T., Hara, K., Ikeuchi, K., 2003. Polarization-based Inverse Rendering from a Single View. *IEEE Int. Conf. on Computer Vision*, Nice, France, vol. II, pp. 982-987.

Nayar, S. K., Ikeuchi, K., Kanade, T., 1991. Surface Reflection: Physical and Geometrical Perspectives. *IEEE Trans. on Pattern Analysis and Machine Intelligence*, 13(7), pp. 611-634.

Powell, M. J. D., 1970. A Fortran Subroutine for Solving Systems of Nonlinear Algebraic Equations," *Numerical Methods for Nonlinear Algebraic Equations*, P. Rabinowitz, ed., Ch.7.

Rahmann, S., Canterakis, N., 2001. Reconstruction of Specular Surfaces using Polarization Imaging. *Int. Conf. on Computer Vision and Pattern Recogntion*, Kauai, USA, vol. I, pp. 149-155.

Wöhler, C., Hafezi, K., 2005. A general framework for three-dimensional surface reconstruction by self-consistent fusion of shading and shadow features. *Pattern Recognition*, 38(7), pp. 965-983.

Wolff, L. B., 1991. Constraining Object Features Using a Polarization Reflectance Model. *IEEE Trans. on Pattern Analysis and Machine Intelligence*, 13(7), pp. 635-657.